

Pump absorption and temperature distribution in erbium-doped double-clad fluoride-glass fibers

Martin Gorjan,^{1,2*} Marko Marinček^{2,3}, and Martin Čopič,^{1,3}

¹Laboratory for Quantum Optics, Faculty of Mathematics and Physics, University of Ljubljana, Jadranska 19, 1000 Ljubljana, Slovenia

²Fotona d.d., Stegne 7, 1210 Ljubljana, Slovenia

³Department for Complex Matter, Institute Jožef Stefan, Jamova cesta 39, 1000 Ljubljana, Slovenia

*martin.gorjan@fotona.com

Abstract: We investigate diode pump absorption and temperature distribution in three erbium-doped double-clad fluoride fibers. Absorption is measured via fluorescence intensity and temperature distribution is measured with thermal imaging. Ray-tracing calculations of absorption and heat-equation modeling of temperature distribution are also conducted. We found excellent agreement between measurements and calculations for all fibers. Results indicate that erbium-doped fluoride fiber lasers have already reached maximum output powers allowed under natural convection cooling, with fiber end being the most critical. We propose cooling and fiber design optimizations that may allow an order-of-magnitude further power-scaling.

©2009 Optical Society of America

OCIS codes: (060.2410) Fibers, erbium; (060.2280) Fiber design and fabrication; (140.3510) Lasers, fiber; (140.6810) Thermal effects

References and links

1. M. O'Connor, V. Gapontsev, V. Fomin, M. Abramov, and A. Ferin, "Power Scaling of SM Fiber Lasers toward 10kW," in *Conference on Lasers and Electro-Optics/International Quantum Electronics Conference*, OSA Technical Digest (CD) (Optical Society of America, 2009), paper CThA3.
2. J. Limpert, F. Roser, S. Klingebiel, T. Schreiber, C. Wirth, T. Peschel, R. Eberhardt, and A. Tünnermann, "The Rising Power of Fiber Lasers and Amplifiers," *IEEE J. Sel. Top. Quantum Electron.* **13**(3), 537–545 (2007).
3. S. D. Jackson, T. A. King, and M. Pollnau, "Modelling of high-power diode-pumped erbium 3 μ m fibre lasers," *J. Mod. Opt.* **47**(11), 1987–1994 (2000).
4. M. Pollnau, S. D. Jackson, "Energy Recycling Versus Lifetime Quenching in Erbium-Doped 3- μ m Fiber Lasers," *IEEE J. Quantum Electron.* **38**(2), 162–169 (2002).
5. X. Zhu, and R. Jain, "Numerical analysis and experimental results of high-power Er/Pr:ZBLAN 2.7 microm fiber lasers with different pumping designs," *Appl. Opt.* **45**(27), 7118–7125 (2006).
6. B. Srinivasan, J. Tafoya, and R. Jain, "High-power "Watt-level" CW operation of diode-pumped 2.7 μ m fiber lasers using efficient cross-relaxation and energy transfer mechanisms," *Opt. Express* **4**(12), 490–495 (1999).
7. T. Sandrock, D. Fischer, P. Glas, M. Leitner, M. Wrage, and A. Diening, "Diode-pumped 1-W Er-doped fluoride glass M-profile fiber laser emitting at 2.8 μ m," *Opt. Lett.* **24**(18), 1284–1286 (1999).
8. S. D. Jackson, T. A. King, and M. Pollnau, "Diode-pumped 1.7-W erbium 3- μ m fiber laser," *Opt. Lett.* **24**(16), 1133–1135 (1999).
9. X. Zhu, and R. Jain, "Compact 2 W wavelength-tunable Er:ZBLAN mid-infrared fiber laser," *Opt. Lett.* **32**(16), 2381–2383 (2007).
10. X. Zhu, and R. Jain, "10-W-level diode-pumped compact 2.78 microm ZBLAN fiber laser," *Opt. Lett.* **32**(1), 26–28 (2007).
11. A. Liu, and K. Ueda, "The absorption characteristics of circular, offset and rectangular double-clad fibers," *Opt. Commun.* **132**(5-6), 511–518 (1996).
12. V. Doya, O. Legrand, and F. Mortessagne, "Optimized absorption in a chaotic double-clad fiber amplifier," *Opt. Lett.* **26**(12), 872–874 (2001).
13. P. Leproux, S. Février, V. Doya, P. Roy, and D. Pagnoux, "Modeling and Optimization of Double-Clad Fiber Amplifiers Using Chaotic Propagation of the Pump," *Opt. Fiber Technol.* **7**(4), 324–339 (2001).
14. S. Bedö, W. Lüthy, and H. P. Weber, "The effective absorption coefficient in double clad fibers," *Opt. Commun.* **99**(5-6), 331–335 (1993).
15. D. C. Brown, and H. J. Hoffman, "Thermal, Stress, and Thermo-Optic Effects in High Average Power Double-Clad Silica Fiber Lasers," *IEEE J. Quantum Electron.* **37**(2), 207–217 (2001).

16. D. J. Coleman, and T. A. King, "Pump induced thermal effects in high power Tm^{3+} and $\text{Tm}^{3+}/\text{Ho}^{3+}$ cladding-pumped fibre lasers," *Meas. Sci. Technol.* **14**(7), 998–1002 (2003).
 17. L. Li, H. Li, T. Qiu, V. L. Temyanko, M. M. Morrell, A. Schülzgen, A. Mafi, J. V. Moloney, and N. Peyghambarian, "3-Dimensional thermal analysis and active cooling of short-length high-power fiber lasers," *Opt. Express* **13**(9), 3420–3428 (2005).
 18. Y. Jeong, S. Baek, P. Dupriez, J.-N. Maran, J. K. Sahu, J. Nilsson, and B. Lee, "Thermal characteristics of an end-pumped high-power ytterbium-sensitized erbium-doped fiber laser under natural convection," *Opt. Express* **16**(24), 19865–19871 (2008).
 19. H. W. McAdams, *Heat Transmission*, (McGraw-Hill, 3rd edition, 1954).
-

1. Introduction

Recent advances in fiber design and manufacturing together with ready availability of powerful diode sources with very high radiances have made possible single-mode fiber lasers with multi-kilowatt output powers [1]. Such lasers are based on rare-earth-doped double-clad silica fibers with low quantum defects and low doping concentrations, making for relatively little heat generation that is spread over long fiber lengths [2]. The silica-glass fiber core and polymer coatings can withstand high temperatures during operation, so thermal loads well in excess of 20 W/m are possible without complex thermal management schemes.

Erbium-doped fiber lasers, however, have high quantum defects and are thus much more prone to thermal ill-effects that prevent them such power-scaling. Fluoride-glass fibers pose a special challenge because of their ionic-bond nature, material properties and high doping concentrations needed for efficient laser operation. Despite substantial theoretical [3–5] and experimental efforts [6–8] they have only reached watt-level stable operation [9]. The highest output power reported was nearly 10 W, albeit with very unstable operation and high risk of damage to the fiber [10]. While the reasons are suspected to be pump and temperature related, until now not much work has been done to investigate the pump and temperature distributions in erbium-doped double-clad fluoride-glass fibers.

Diode pump absorption in double-clad fibers [11, 12] and its influence on fiber amplifier operation [13] has been studied theoretically, but experimental data has been scarce [14]. Fiber temperature and its effect on laser operation, on the other hand, have been investigated for some fiber laser types. Thorough theoretical analysis has been done for Yb-doped silica fibers [15]. Measurements of the pump-induced temperature distribution were done using thermal imaging in Tm-doped silica and ZBLAN fibers [16], fluorescence spectrum analysis [17] and also by using fiber Bragg gratings sensor [18] on Er/Yb silica fiber laser.

We hereby report a thorough experimental and theoretical investigation of the pump absorption and temperature distribution in erbium-doped double-clad fluoride-glass fibers. First, we present an innovative technique for measuring pump absorption via fluorescence intensity that may also be applicable to some other doping types. It enabled us to use imaging methods for the first time to capture both pumping and fiber temperature in order to examine in detail the pumped fiber end in addition to the bulk of the fiber. Using three fibers of the same doping concentration but varying in core/cladding geometry made it possible to show unambiguously the close correlation between pump absorption and temperature up to the very tip of the fiber and validate the model calculations at the same time. Next, we introduce a general relation for the temperature of the core at the fiber end that accounts for the interplay of pump absorption, fiber geometry, heat transfer mechanisms and laser operating parameters. We find it instrumental in the fiber design optimization for thermal dissipation and results on its basis indicate that end-pumped erbium-doped fluoride-glass fiber lasers may have already reached the maximum output powers attainable under natural convection cooling. Finally, we introduce the so called conductive limit and show that there is still much room for improvement in lowering the core temperatures and thus maybe further power-scaling up to 100 W-level of the average output powers, which we deem the fundamental thermal limit.

2. Experimental setup

We performed the measurements of pump absorption and temperature distribution on the experimental setup that included a fiber-coupled pump diode source JOLD-75-CPXF-2P-

iTEC from Jenoptik Laserdiode GmbH emitting at 975 nm. Its output was coupled to 400 μm 0.22 NA silica fiber from CeramOptec and was imaged with two off-axis gold-coated parabolic mirrors from Edmund Optics that provided virtually aberration-free reduced image of the pumping fiber exit at the entrance of the studied fluoride fibers. The experimental fluoride fibers consisted of three 4 m long samples manufactured by FiberLabs, Inc. They were all double-clad designs with 6% ErF_3 doped ZBLAN core, undoped HBLAN cladding and UV curable polyacrylate coating that also acted as cladding for the pump light. Core/cladding had numerical apertures of 0.12/0.5 and the geometry data is given in Table 1. Fiber preparation included polishing and mounting both ends in fiber chuck model BFC300 from Siskiyou in such a way that ~ 2 cm of the fiber ends were protruding. One end of the fiber (referred to as the fiber end) was positioned in front of the pump spot and the bulk of the fiber was coiled on a standard spool 33 cm in diameter.

Table 1. Geometry of Er-doped double-clad ZBLAN fibers used in our measurements

Fiber	Core	Cladding	Coating
30/300/CC	30 μm	300 μm circular	430 μm
30/350/D	30 μm	350 μm D-shape	480 μm
20/350/D	20 μm	350 μm D-shape	430 μm

3. Pump absorption

3.1 Fluorescence intensity measurements

It is well known that erbium-doped fiber core fluoresces vigorously when under pump excitation; the most prominent are two green bands (522 and 544 nm) but the exact fluorescence spectrum generally depends on many factors like host type and core temperature [17]. We have constructed a special positioning tool to measure the side-emission spectrum of all our fibers and its dependence on the fiber position as well as the pump power using fiber-coupled UV/Vis spectrometer Ocean Optics HR2000+ as shown in Fig. 1. We have observed that overall integrated fluorescence intensity (excluding the scattered pump at 975 nm) recorded on every one position is exactly proportional to the pump power. This implied that integral fluorescence intensity can be used to locally probe for the pumping of the fiber core with great spatial resolution and can even be used on the fiber end. As the local pumping is expected to be proportional to the local absorption in the core, the length dependence of the absorption can thus be measured. Such technique is superior to a simple cut-back experiment, which is destructive for the fiber, it can be tedious and works well only for longer fiber lengths so that it cannot be used on the fiber end, which was of greatest interest to us.

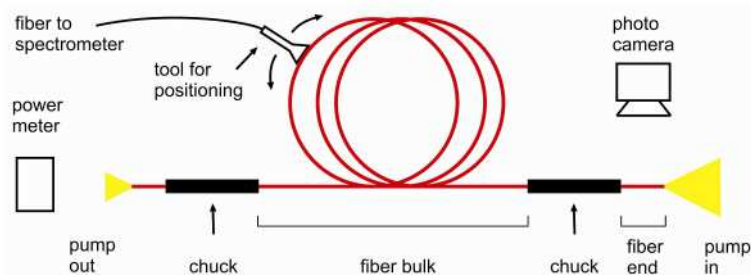


Fig. 1. Setup for measuring the pump absorption at two locations in a free fiber configuration.

We have measured the absorption via fluorescence on the bulk of all the fibers in 25 cm intervals. The resulting normalized intensity as a function of position is plotted in Fig. 2 (a), where exponential-like decay is evident. We have measured the residual pump power coming from the other end of the fiber using Coherent FieldMaxII power meter as depicted on Fig. 1. The absorption on full length (4 m) was 99% for D-shaped fibers and 80% for the concentric circular fiber. For the reference we have also performed a cut-back experiment on the CC

fiber on four lengths (0.8 m, 1.3 m, 2.6 m and 4 m). The obtained results did agree with the fluorescence method as can be seen in Fig. 2 (b) where the fluorescence intensity and absorption in the fiber are shown. Because the full absorption is only 80% that means that 20% of the pump power still propagates in the fiber cladding but does not overlap with the core anymore after first 4 m of the fiber length. This is in contrast to theoretical calculation [11], which predicts that only about 30% of the pump power can be absorbed in the core. We suspect the difference is due to the geometrical and material inhomogeneity of the real fiber.

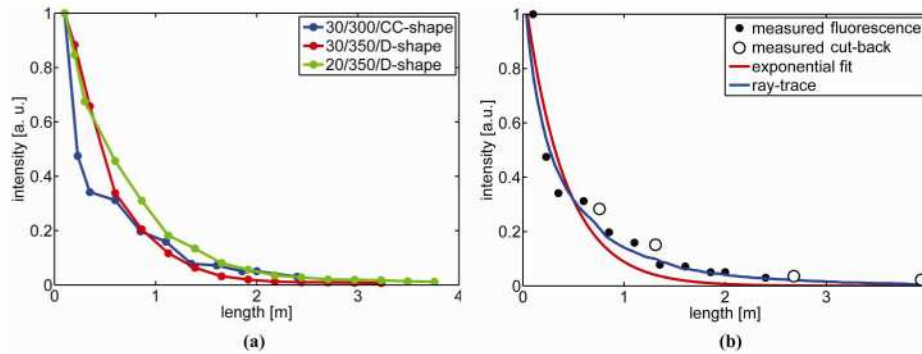


Fig. 2. (a) Measured fluorescence intensity for all fibers on the bulk and (b) measured/calculated pump absorption for 30/300/CC fiber.

The fiber ends were treated separately by taking photographs with Canon EOS 300D digital camera equipped with macro lens. They were stored in RAW format and analyzed in Matlab software package, where integration over core diameter was performed. The results are plotted in Fig. 3 (a), where the plots for individual fibers are artificially arranged on vertical scale to match the calculated results in Fig. 3 (b) as no calibration was performed.

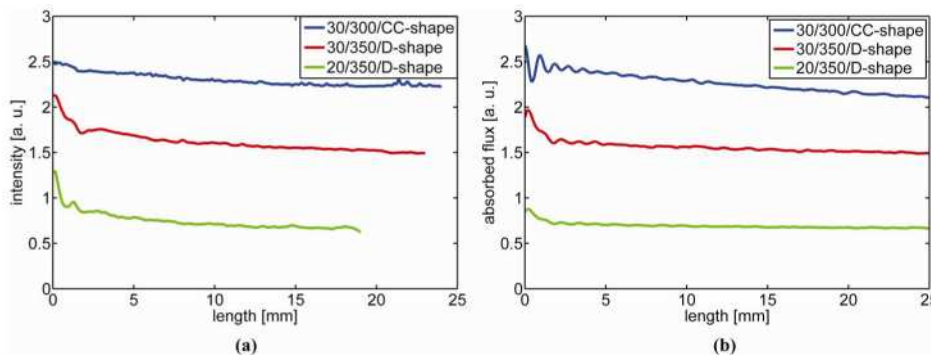


Fig. 3. (a) Measured fluorescence intensity on fiber ends and (b) ray-trace calculated pump absorption.

Finally, we have constructed a fiber laser resonator by putting a gold-coated spherical mirror at the non-pumped fiber end while the 4% Fresnel reflection acted as an output coupler as depicted in Fig. 4. A dichroic mirror was used to separate the pump and laser radiation. The laser had a threshold of 400 mW pump power, 21% slope efficiency and emission at around 2780 nm. We repeated all the measurements on a D-shaped fiber; the intensity of the fluorescence was a bit diminished, but the distributions remained exactly the same.

3.2 Beer's law and ray-trace calculations

The pump absorption in rare-earth-doped double-clad fibers with chaotic propagation can be approximated by Beer's law of absorption [12–14] with the effective coefficient of absorption:

$$\alpha = \alpha_m \frac{\pi r_c^2 NA_c}{A_d}. \quad (1)$$

Where α_m is the material absorption, r_c and NA_c are radius and numerical aperture of the core and A_d is the cladding area. If the pump light intensity were homogeneously distributed in the core and cladding, the effective absorption coefficient would be proportional to the ratio of the respective areas. The additional factor NA_c takes care of the fact that the intensity of the pump radiation in the core is higher due to the guiding effect of the core.

We made a fit on the measured full length using absorption coefficient from Eq. (1) and fiber geometry parameters from Table 1. For both D-shaped fibers the fit was very good, while less so for circular fiber as can be seen in Fig. 2 (b) which was already observed [14]. The resulting value of the material absorption is $\alpha_m = 1.6 \text{ mm}^{-1}$.

In search of a better model we have also conducted ray-trace calculations in Zemax EE optical design software using fiber parameters from Table 1. The results were found in excellent agreement with the measurements for all three fibers and both for the fiber bulk and the fiber ends: Fig. 2 (b) displays the agreement with the observed non-exponential decay for circular fiber, while Fig. 3 (b) displays the agreement for the fiber ends. We have also employed the ray-tracing analysis to test the validity of Eq. (1) and it was fully confirmed.

4. Temperature distribution

4.1 Thermal imaging measurements

The fiber temperatures were measured using FLIR Systems ThermoCAM P45 thermal imaging camera with macro lens operating in 8-12 μm wavelength region; the measurements were conducted on all fibers in free-end and laser resonator configuration on both the fiber bulk and fiber end as depicted on Fig. 4. The camera was auto-calibrated with temperature resolution of 0.1 K and spatial resolution of 100 μm . The emissivity parameter was set to the value for polyacrylate coating ($e = 0.92$), and we have additionally checked the validity of the measured temperatures by contrast method which were in full agreement.

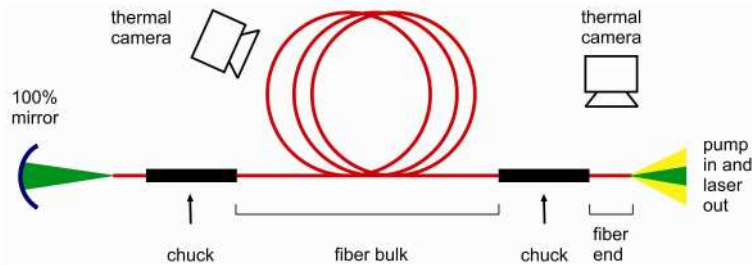


Fig. 4. Setup for measuring the temperature distribution at two locations in a laser resonator configuration.

The raw recorded thermal images for the fiber end are shown in Fig. 5; even with the pump off the fiber can still be seen because the surroundings have lower emissivity. On the bulk of the fiber we recorded just a few points along the fiber length (not shown) and they were all found in good correlation with the measured pump absorption shown in Fig. 2 (a). For the fiber end the thermal image was analyzed in Matlab software package but now the integration was done over the full diameter of the fiber; the reason is the fiber coating/cladding opacity in the imaging wavelength range as can be seen in Fig. 5.

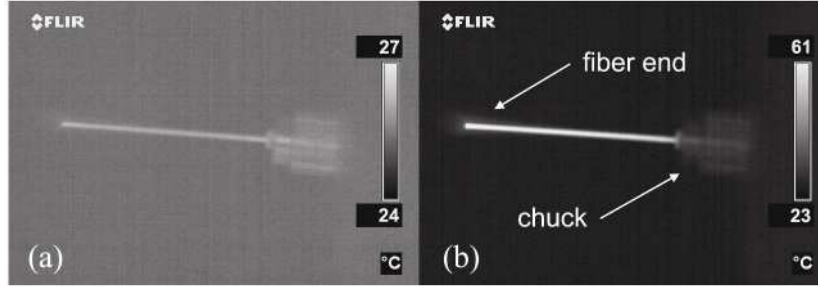


Fig. 5. IR image of the fiber end with (a) pump off and (b) pump on.

The obtained results are plotted in Fig. 6 (a) and were found in good correlation with the measured pump absorption from Fig. 3 (a). Small temperature rise on the far right was caused by fiber chuck jaws restricting the air flow. Only the temperature of the 30/350/D fiber was a bit lower than expected, but even that discrepancy is explained in the next subsection. We did not observe much difference between the measurements on free-end and laser resonator configurations; the temperature distributions were exactly the same, while the fiber laser did show somewhat lower temperatures, but only of about 10%. This is a bit surprising when considering the observed 21% slope efficiency of the laser operation.

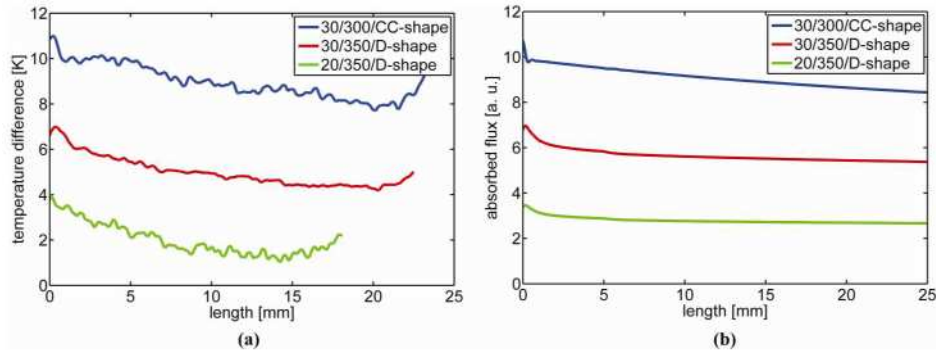


Fig. 6. (a) Measured surface temperatures for fiber ends under 0.7 W pump and (b) calculated surface temperatures from heat-equation model.

4.2 Heat equation model

Fiber temperature during operation is a 3D boundary value problem with the core acting as a heat source, but it can be simplified to a 1D model [15]. The huge difference between the fiber length and diameter causes heat to flow almost exclusively in the radial direction. Moreover, with the possible exception of fibers with highly eccentric core, the radial symmetry can be applied. The fiber temperature can then be modeled by the radial heat equation:

$$-\frac{k(r)}{r} \frac{\partial}{\partial r} \left(r \frac{\partial T(r)}{\partial r} \right) = \begin{cases} Q_h; & 0 \leq r \leq r_c \\ 0; & r_c \leq r \leq r_g \end{cases} \quad (2)$$

Where $k(r)$ is thermal conductivity of glass and polymer, Q_h is the heat source density in the core and $r_c/r_d/r_g$ are the core, cladding and coating radii. With Newton's law of cooling as the boundary condition, Eq. (2) can be solved analytically and the temperature calculated using heat transfer coefficient of the fiber's outermost layer, in our case the coating:

$$h = h_{nc} + h_{rad} = h_{nc}^0 \left(\frac{r_g}{r_{nc}^0} \right)^{-2/3} + 4\pi\sigma T_{amb}^3. \quad (3)$$

The two terms in Eq. (3) account for natural convection h_{nc} and radiation h_{rad} . The natural convection term is commonly given [19] in form of a power-law with different powers for different dimensional regions of interest. Because we were unable to find the proper region of interest, which in our case is the fiber diameter, we obtained the relation on the right-hand side of Eq. (3) by means of computational fluid dynamics with the values $h_{nc}^0 = 50 \text{ W}/(\text{m}^2\text{K})$ and $r_{nc}^0 = 250 \text{ }\mu\text{m}$. The radiation term on the right-hand side of Eq. (3) is obtained by linearization of the Stefan-Boltzmann law around the ambient temperature and is about $10 \text{ W}/(\text{m}^2\text{K})$. It is interesting to note that the natural convection term depends significantly on the dimensions of the fiber; while it is about $10 \text{ W}/(\text{m}^2\text{K})$ for diameters larger than a millimeter, it is $50 \text{ W}/(\text{m}^2\text{K})$ for $250 \text{ }\mu\text{m}$ and more than $100 \text{ W}/(\text{m}^2\text{K})$ for $125 \text{ }\mu\text{m}$ diameter fibers.

The model can be used to calculate the radial dependence of temperature at any given position along the fiber length and the pump absorption measurement or calculation can be used to provide the axial dependence; this is applicable even down to a millimeter scale, which is also evident when comparing Fig. 3 (a) with Fig. 6 (a). For single-end pumping that is considered here, the highest temperature is obviously at the very tip of the pumped fiber end. The solution for temperature difference against ambient reference for $1 \text{ W}/\text{m}$ thermal load is plotted in Fig. 7. The whole fiber is almost at an equal temperature, which is substantially higher than the ambient. Using ray-trace results as the axial dependent heat source, we calculated the temperatures for the fiber ends, which are plotted on Fig. 6 (b). Interestingly, we found that thicker coating can sometimes lower the fiber surface and even core temperature by increasing the dissipation surface. This was actually observed in the case of 30/350D fiber and can be observed from Fig. 6 (a).

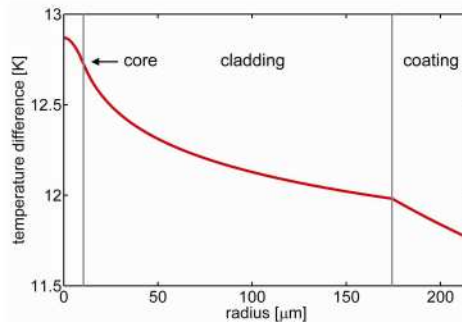


Fig. 7. Calculated fiber temperature for $1 \text{ W}/\text{m}$ thermal load.

5. Fiber design optimization

Besides increasing the efficiency of operation, which proved to be very difficult to achieve with erbium-doped fluoride-glass fiber lasers [7–10], simply increasing the pump powers is the most straightforward way to achieve greater laser output powers. However, this invariably increases the fiber temperatures as well. It is clear from the previous sections that fiber core at the pumping end is under the greatest thermal load, which can hinder the laser performance and limit the attainable laser power. Indeed, it has already been reported [10, 16] that the thermal breakdown and melting of the fiber tip seems to be the current barrier for some fluoride-glass fiber lasers, including the erbium-doped one.

Generally two things can be done to decrease the fiber temperatures: to arrange for a better heat dissipation (thus increasing the heat transfer coefficient h) or optimizing the fiber design (thus decreasing the generated heat density Q_h). In any case, the thermal conductivity of the fiber itself ultimately provides the limit for heat dissipation, and only fiber design can provide

any further optimization. To study the interrelated effects of the fiber design on the pump absorption and heat dissipation at the tip of the fiber end we have applied absorption model from Eq. (1) as the heat source in thermal model from Eq. (2) and Eq. (3) to get the following expression for temperature rise in the center of the fiber end tip:

$$\Delta T_c = P_{\text{pump}} \frac{(1-\eta)\lambda\alpha_m V_c}{8\pi^2 k} \frac{r_c}{r_d^2} \left[1 + 2 \log\left(\frac{r_d}{r_c}\right) + \frac{2k}{hr_d} \right]. \quad (4)$$

Where P_{pump} is the incident pump power, α_m material absorption in the fiber core, k thermal conductivity of the fiber, V_c the V-number of the core for laser wavelength λ and η the slope efficiency of the laser operation. The first part of the Eq. (4) covers the laser operating parameters and some implications are immediate: increasing the laser slope efficiency does decrease the temperature, but not necessarily so if the material absorption, i.e. because of higher doping concentration, is increased as well; smaller V-numbers are better, because of the decreased size and numerical aperture of the core, so single-mode fibers are preferred in this regard as well. The second part of the Eq. (4) covers the fiber geometry and includes only the core/cladding radii with the coating omitted for simplicity as if it is thin enough it does not have any significant influence anyway (see Fig. 7). The implications here are not as evident with the exception of identification of the heat transfer coefficient as the effective bottleneck (see also Fig. 7).

In order to further clarify the matters concerning the fiber geometry we used single-mode condition ($V_c = 2.405$), pump power $P_{\text{pump}} = 1$ W, the measured material absorption coefficient $\alpha_m = 1.6 \text{ mm}^{-1}$ and laser operating parameters $\lambda = 2.78 \text{ }\mu\text{m}$ and $\eta = 0.21$; the thermal conductivity of the ZBLAN glass is $k = 0.63 \text{ W/mK}$. We considered two limits: the convective limit that is imposed by Eq. (3) and represents horizontally oriented fiber end tip in free air, and the conductive limit that is imposed by setting h to infinity and represents the thermal resistance of the fiber itself. The latter may be practically approached, e.g. by putting the fiber in good thermal contact with a cold-plate, and while this is easy to do on the bulk of the fiber it seems like a much greater challenge for the pumped fiber end tip as any stray pump light could cause serious problems. The resulting temperatures as functions of the cladding radius are plotted in Fig. 8. It can be noted that larger cladding radii produce lower, while larger core radii produce higher temperatures for both limits as thermal load is spread over longer/shorter fiber lengths.

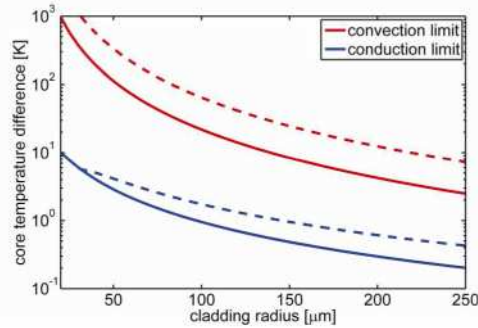


Fig. 8. Core temperatures for 10 μm (solid) and 30 μm (dashed) core radii.

To estimate the ultimate attainable power before incurring thermal damage to the core, we have substituted the relation between the pump and laser power $P_{\text{pump}} = P_{\text{laser}}/\eta$ to the Eq. (4) and solved for the laser power. The following expression was obtained:

$$P_{\text{laser}}^{\text{max}} = \Delta T_c^{\text{max}} \frac{8\pi^2 \eta k}{(1-\eta)\lambda\alpha_m V_c} \frac{r_d^2}{r_c} \left[1 + 2 \log\left(\frac{r_d}{r_c}\right) + \frac{2k}{hr_d} \right]^{-1}. \quad (5)$$

Where ΔT_c^{\max} now represents the highest temperature difference against given reference that the fiber (core) material can withstand. We used the same fiber and laser operating parameters as above, the transition temperature of ZBLAN glass $T_g = 535$ K as the maximum and 300 K as the reference ambient temperature. The output powers are now plotted as the functions of core radius in Fig. 9 where it can be noted again that lower core radii enable higher output powers. In this case, however, the optical breakdown limit also has to be taken into account; the measured value [10] of 25 MW/m^2 was taken and the maximum power in the optical limit is plotted in Fig. 9 as well. The intersections between the optical and thermal limit now provide the final estimation of the maximum attainable power of erbium-doped fluoride-glass fiber lasers that operate near $3 \mu\text{m}$ and with efficiency close to 20%. Free-air operation seems to be limited to 10 W level and core radii around $5 \mu\text{m}$ the most appropriate, while with proper cooling solution the ultimate limit seems to be in the 100 W range with core radii between 10 and $15 \mu\text{m}$ the most appropriate. We find the highest power yet reported [10]: 9 W from a single-mode $7.5 \mu\text{m}$ radius core and $\sim 200 \mu\text{m}$ cladding radius fiber suspended in free-air in good agreement with these predictions.

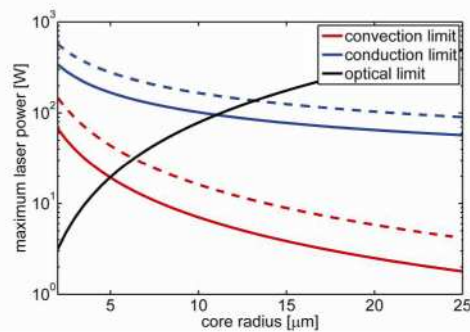


Fig. 9. Laser power for $150 \mu\text{m}$ (solid) and $200 \mu\text{m}$ (dashed) cladding radii.

6. Conclusion

In this paper we presented measurements of the fiber pump absorption based on fluorescence intensity, which were found in excellent agreement with our ray-trace calculations modeled in commercial optical software, providing better results than the Beer's law approximation. Temperature distributions were measured with thermal imaging and intimate relation with the pump absorption was established. Fiber temperature was also modeled with heat-equation, which allowed analysis of the fiber design optimizations for lowest running temperatures and highest attainable output powers with given laser slope efficiency. We conclude that the end-pumped erbium-doped fluoride fiber lasers with currently demonstrated efficiencies of 20% may have effectively reached the natural convection limit and thermal management for the fiber up to the very tip would be needed for further power-scaling.